Identification and Control of a Grating-Stabilized External-Cavity Diode Laser

W. Weyerman, *Student Member, IEEE*, B. Neyenhuis, J. Archibald, M. Washburn, D. Durfee, and S. Warnick, *Member, IEEE*

***Abstract*—Diode lasers have many useful properties and have found a variety of uses including CD and DVD players, barcode scanners, laser surgery, water purification, quantum-key cryptography, spectroscopic sensing, etc. Nevertheless, their intrinsic linewidth or the precision of their emitted wavelengths, is not good enough for many cutting-edge applications such as atomic interferometry or high-performance atomic clocks. Using active feedback control, we can narrow the linewidth of a diode laser by not allowing the frequency of emitted light to drift away from a reference value. Nevertheless, such feedback designs are challenging because of a lack of first principles models and difficult sensor dynamics. This brief describes our diode laser system and reports our results identifying the system using black-box techniques, validating the empirical models, and designing controllers to achieve desired performance while preserving stability and satisfying implementation constraints.**

***Index Terms*—Frequency control, identification, linear approximation, proportional control, semiconductor lasers.**

I. Introduction

DIODE lasers have some very unique qualities which have enabled many scientific and technological advances [7]. Compared to other lasers, they are inexpensive, compact, and efficient. They typically require little power and usually do not produce a lot of heat. Their wavelength can be quickly modulated. Diode lasers are also available at many different wavelengths, and a given diode can typically be tuned with temperature and optical feedback over several nanometers. Nevertheless, the wavelengths of the light emitted by a diode laser can be relatively broad and tend to drift over time.

Bare laser diodes do not have the stability and narrow linewidth necessary for many applications such as spectroscopy and laser cooling and manipulation of atoms. Placing the diode in an external cavity can reduce the linewidth of a diode laser, making it suitable for many more applications [7]. The linewidth can be reduced even more by locking the laser to a stable reference cavity. Some of the most stable lasers in the world have been created by actively locking an external-cavity diode laser (ECDL) to an ultra-high finesse optical cavity, [4], [5], [8]. In [4], it is noted that a much smaller linewidth is likely to be achieved through optimized adjustment of the servo amp. Typically, more attention is given to the components of the laser than design of the controller [5], [8].

Manuscript received January 16, 2007; revised July 28, 2007. Manuscript received in final form January 31, 2008. First published June 13, 2008; current version published December 24, 2008. Recommended by Associate Editor J. Lee.

W. Weyerman and S. Warnick are with the IDeA Labs, Department of Computer Science, Brigham Young University, Provo, UT 84601 USA (e-mail: wsweyerman@gmail.com; sean@cs.byu.edu).

B. Neyenhuis, J. Archibald, M. Washburn, and D. Durfee are with the Department of Physics and Astronomy, Brigham Young University, Provo, UT 84601 USA.

Digital Object Identifier 10.1109/TCST.2008.921812

We have constructed an external-cavity diode laser to use as the oscillator in a next-generation optical-frequency atomic clock. To achieve the extreme level of stability required for this application, we have mounted the laser in a heavy, mechanically isolated box with a large thermal mass, have developed high-stability, low noise current sources, etc. To cancel out environmental noise and drift, the laser is locked to an ultra-high finesse optical cavity, as mentioned above. Using this cavity, we generate an error signal which we can use for active feedback control of the laser to keep the wavelength from drifting away from its reference value.

In this brief, we describe our laser system and discuss the sensor system that compares the laser's wavelength to a reference to generate an error, and define notation for the corresponding closed-loop system. We then describe our identification process for the system, which is necessarily black-box and closed-loop. In this process, we identify two models for the laser system and characterize the frequency response of an additive noise disturbance. Finally, we validate our models by comparing the experimental and theoretical responses to a new controller design. This experiment allows us to identify bandwidth limitations due to the presence of unmodeled dynamics, thereby characterizing the limitations of our empirical black-box models. We test these limits by discussing a controller that theoretically should stabilize the system and deliver excellent performance, but which excites these unmodeled dynamics. The resulting experimental implementation is unstable, demonstrating the need to avoid the unmodeled dynamics. We finally discuss a controller that avoids exciting the unmodeled dynamics while delivering acceptable performance. The implementation of this controller is stable and provides the expected performance for this system.

II. System Description

Our laser system consists of two main components, the external cavity diode laser (ECDL), a laser diode, and an external cavity which assists in stabilizing the wavelength of the light, and the sensor. The ECDL configuration that we are using is the Littrow configuration as illustrated in Fig. 1. Our configuration is explained in detail in [6]. In spite of the external cavity diode laser's ability to generate a strong, sharply defined optical mode, thermal, electrical, and mechanical noise cause the color or wavelength of this mode to drift over time. This makes the ECDL unsuitable for applications such as atomic interferometry and high performance atomic clocks. However, the ECDL configuration enables the possibility of stabilizing the drifting wavelength using feedback control.

The wavelength of the light cannot be measured directly, so we use the Pound–Drever–Hall method [1]–[3] to generate a dc error signal based on the deviations of the laser's wavelength from a reference wavelength. A diagram of our setup is shown in

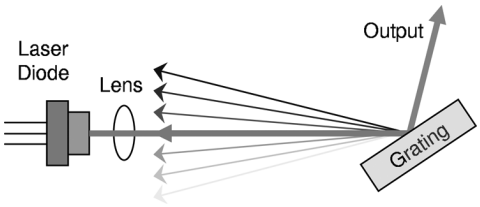

Fig. 1. Littrow configuration. Changing the wavelength of the laser is accomplished by either rotating the grating, sliding the grating to change the length of the cavity, or changing the effective refractive index of the diode.

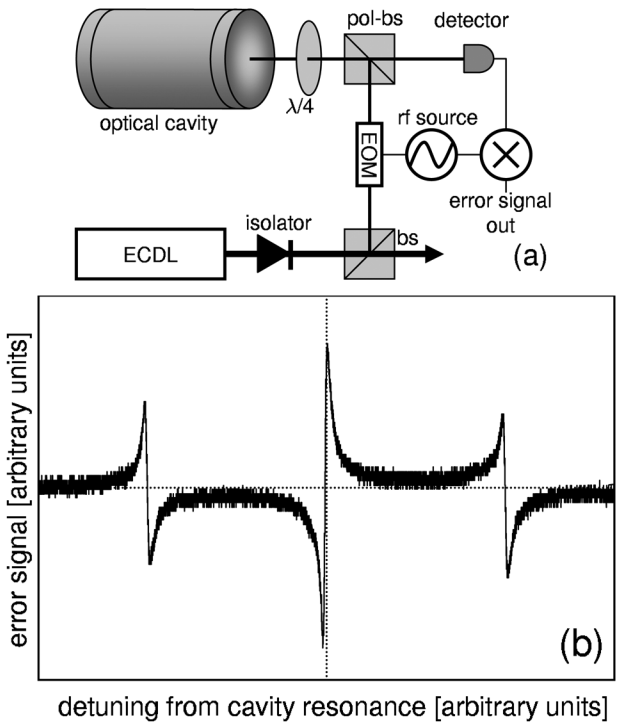

Fig. 2. Pound–Drever–Hall method of generating an error signal between a laser's emission and a desired wavelength, characterized by a particular optical cavity. (a) Diagram of our setup. (b) Magnitude of the error signal generated by our setup is shown as the wavelength of the laser is swept through a cavity resonance. The wavelength of the laser matches the cavity resonance in the center of the plot where the magnitude crosses zero; this is where the laser's output matches the reference. There is a small region centered around this point where the error signal behaves linearly. The slope and width of this section is determined by the fidelity of the cavity: a higher fidelity cavity creates a steeper and more narrow region. Just beyond these wavelengths, error rapidly approaches zero, causing the system to lose observability and effectively go to sleep. If the laser's wavelength is far enough from equilibrium, the error switches sign and the controller will drive the laser away from equilibrium.

Fig. 2(a). An illustration of the magnitude of the error signal produced by the Pound–Drever–Hall sensor as the laser is detuned from cavity resonance is shown in Fig. 2(b). The Pound–Drever–Hall mechanism behaves linearly only for a tiny band of wavelengths near the reference command. Outside of this region, the error signal quickly goes to zero even though the laser wavelength is not close to the reference command. Once this happens, the system will effectively lose observability since the sensor will report zero error from the desired wavelength when, in fact, the error may be significant.

A block diagram of the feedback system is given in Fig. 3. We will specify five systems, P, P_L, P_S, W_0, and K, with $P = P_L P_S$. P_L is the ECDL, P_S is the Pound–Drever–Hall

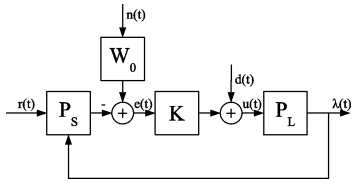

Fig. 3. Diagram of the closed-loop system.

frequency sensor, as described previously. The sensor consists of all the components the light enters after being reflected by the first beamsplitter in Fig. 2(a). The system W_0 shapes the noise entering the system and is determined experimentally. The controller is denoted as K.

Several signals are also represented in Fig. 3. $\lambda(t)$ is the wavelength of the light exiting the laser and is represented in Fig. 2(a) as the light that is not reflected by the first beamsplitter. We want this signal to stay as close as possible to the reference wavelength $r(t)$, which is determined by the length of the optical cavity in the sensor. The signal $e(t)$ is the error as measured by the sensor. The signal $n(t)$ is white noise entering the system, $d(t)$ is an artificial disturbance signal intentionally added by us for system identification, and $u(t)$ is the input to the laser. The signals that we can measure are $d(t)$, $u(t)$, and $e(t)$.

III. Identification of the Laser System

One of the aspects of this system that makes identification difficult is the absence of first principle models for each component that we can easily interconnect and parameterize to create a complete model. Nevertheless, effective controller design demands some understanding and model of the system to guide its development. Thus we turn to black-box identification methods to generate a coarse, linear time invariant control-oriented model of the system. This model will be described in two pieces: the ECDL/PDH system and the noise model.

A. Identification of the ECDL/PDH System

Black-box identification methods are challenging for the ECDL/PDH system because the Pound–Drever–Hall detection technique, which effectively compares the system output with a desired response and generates an error (see Fig. 3), operates linearly in only a very narrow region near equilibrium. Outside this region, the error appears to go to zero when, in fact, it remains decidedly non-zero, and the system effectively loses observability. Moreover, since the amplitude of typical noise in the system easily perturbs it outside this linear regime, it is essential to use feedback to attenuate noise and control the system when collecting measurements. As a result, closed-loop identification is essential, even though we have no models to guide the design of this initial stabilizing controller. Nevertheless, through workbench trial-and-error, we obtained such a controller and were able to subsequently collect data for system identification.

The idea behind our identification experiments was to excite the stabilized, closed-loop system with sinusoids of different frequencies and measure the resulting magnitude and phase of the response. We would then fit these points in the frequency domain with the response of a rational transfer function, and use this transfer function as our model of the system.

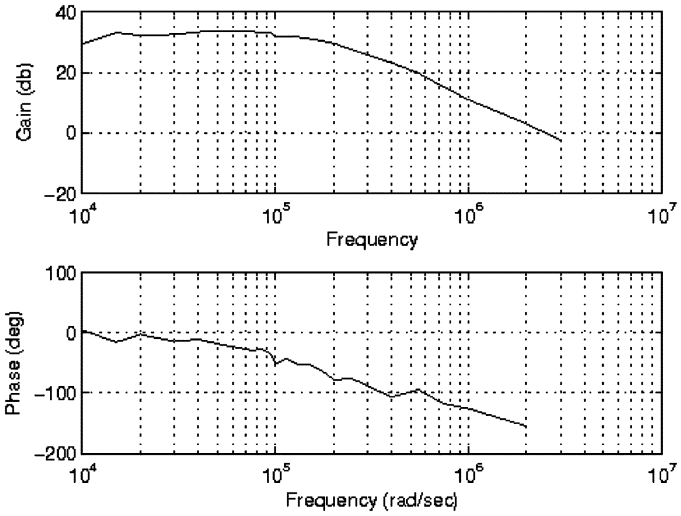

Fig. 4. Magnitude measurements from a single frequency scan to characterize the laser system. At about 10^4 rad/s, we notice some dynamics where the magnitude dips and comes back up. After 10^5 rad/s the magnitude begins to roll off at a rate of 40 dB/dec.

We began by selecting roughly twenty sample frequencies ranging from 1 kHz to 3 MHz. For each frequency, ω, we introduced our sinusoidal disturbance $d(t)$ as an additive perturbation on the current signal, $u(t)$, driving the external-cavity diode laser. We then measured the resulting error signal $e(t)$ produced by the Pound–Drever–Hall detection mechanism. Using a fast Fourier transform on these signals, we were thus able to measure $|U(j\omega)|$ and $|E(j\omega)|$, and calculate $|P_0(j\omega)| = |E(j\omega)|/|U(j\omega)|$. To determine the phase of the laser system, we measured the time delay of the sinusoid, $\delta(\omega)$ from u to e. We then calculated the phase in degrees as $\angle P_0(j\omega) = 360\omega * \delta(\omega)$. Having completed a scan over the entire range of frequencies, we then repeated the experiments 25 times to ensure we captured sufficient data to make meaningful fits and reduce the impact of experimental error.

Fig. 4 shows the measurements obtained for one of the 25 scans. Noting that the system rolls off at 40 db/dec, the simplest model to fit the data would be a second-order system. Fitting such a system, we obtain

$$P_2 = \frac{3.278e12}{(s + 2.53e5)^2}$$

and observe its fit to all of the scan data in Fig. 5(a).

To obtain a higher fidelity model, we note in Fig. 4 the slight dip and hump around 10–20 and 50–60 krad/s, respectively. Using a fourth-order model to capture this feature, we find

$$P_4 = \frac{1.071e13(s^2 + 3.197e4s + 3.044e8)}{(s + 1.674e6)(s + 1.105e5)(s + 3.228e4)(s + 9931)}$$

and observe its fit to all of the scan data in Fig. 5(b).

These models appear to capture much of the dynamic information about the laser system obtained through our black-box identification experiments. In particular, however, we note that the quality of fit of both models appears to deteriorate significantly at frequencies higher than 10^6 rad/s. The second-order model exhibits strong deviations in it's magnitude response, while the fourth-order model exhibits strong deviations in its phase response. We will see later that this high frequency limitation to our models, indicating the presence of unmodeled dynamics in this range, contributes to bounds on our achievable closed-loop performance.

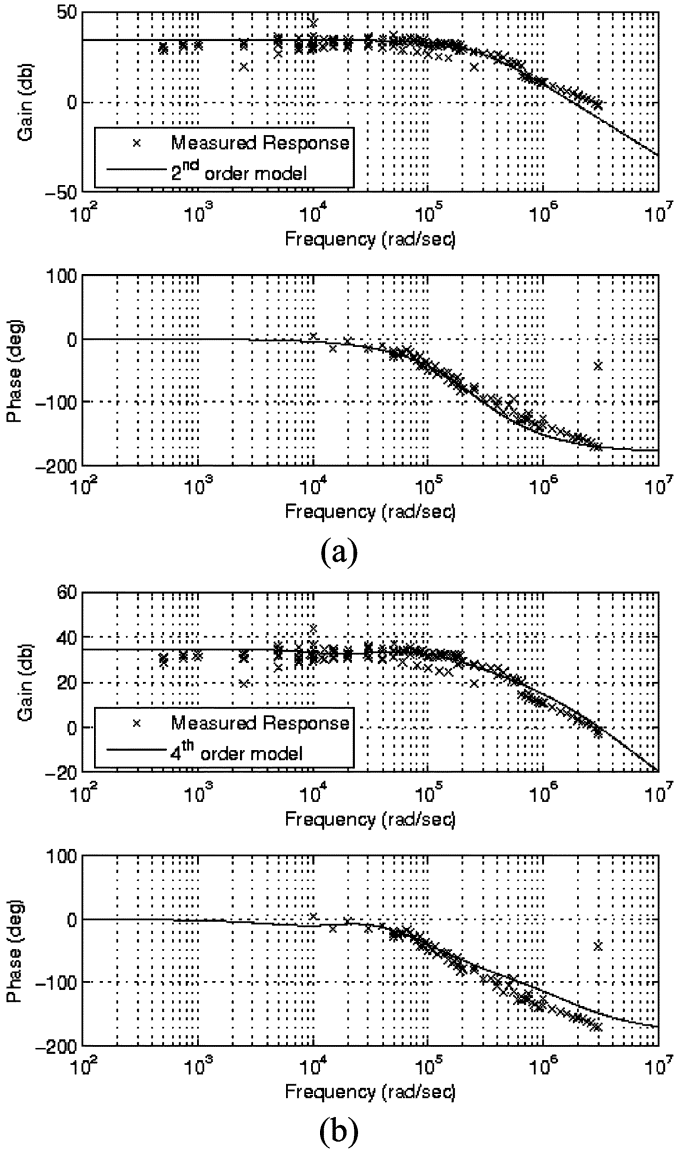

Fig. 5. Open loop models of the ECDL/PDH system plotted against the measured response of the laser from u to e. (a) Second-order model. (b) Fourth-order model.

B. Identification of the Noise Model

Considering discrepancies in the model to be explained by additive noise on the error signal generated by the Pound–Drever–Hall system, we developed a frequency weight model of this discrepancy. Given a stabilizing controller, the idea was that any deviation from equilibrium would be explained by this model. Thus, measuring the error signal when the closed-loop system should be in equilibrium allows us to factor out the impact of the controller, K, and the laser system, P, yielding $W_0 = (1 + PK)E/N$. Here, we assume that n is unit intensity white noise. We repeated this process 30 times to compare the results of a single experiment with the experimental average.

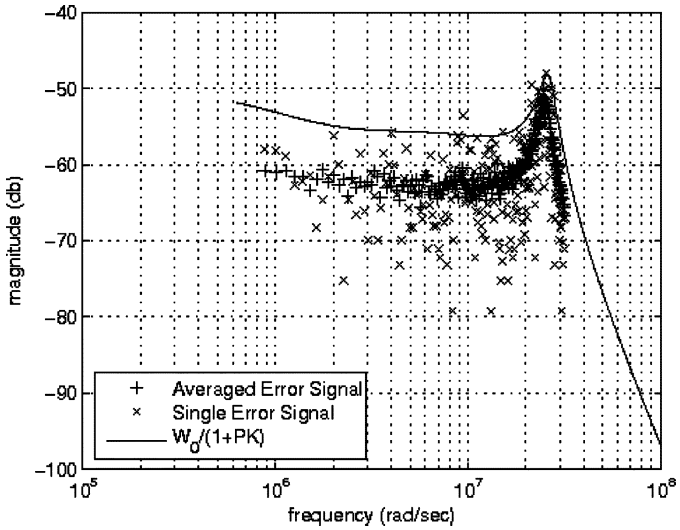

Fig. 6. Frequency weight on noise, W_0, chosen to conservatively cover experimental values.

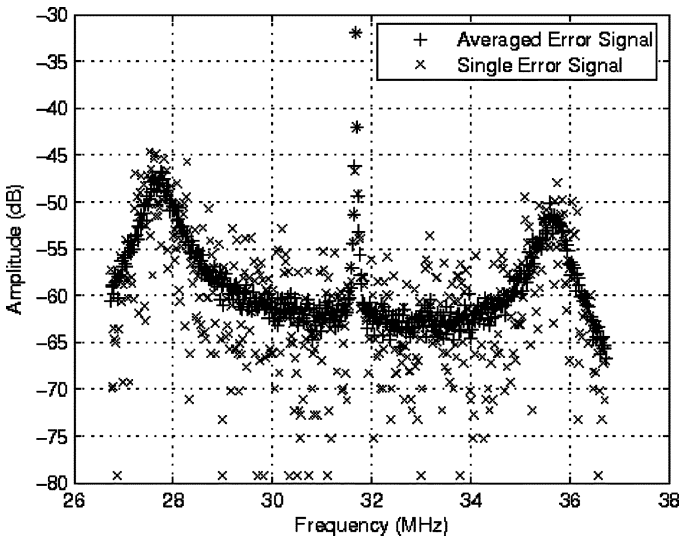

Fig. 7. FFT of the power spectrum of the signal measured at the photodetector while the laser is locked. Note the center spike corresponds to our modulation frequency of about 32 MHz.

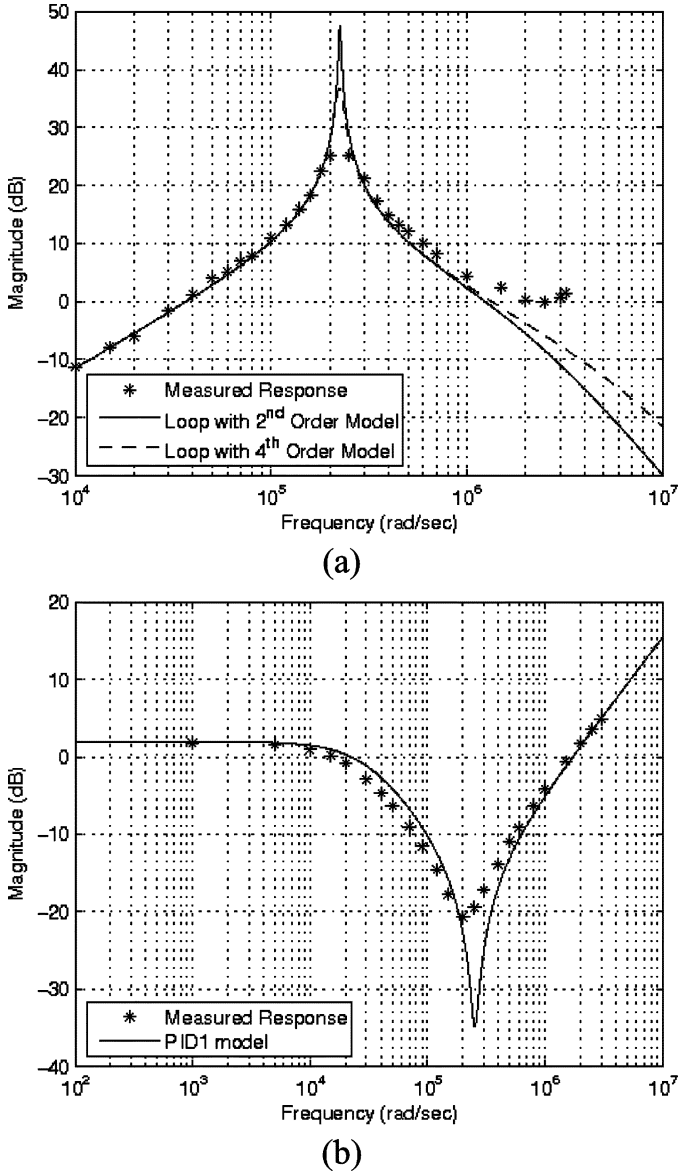

Fig. 8. Measurements with comparisons to our models for PID1. (a) Closed-loop Bode plot from d to e of both models with $K = \mathrm{PID1}$ compared to the measured closed loop response from d to e. (b) Open-loop bode plot of the model of PID1 compared with measured values of the open-loop response of the actual controller.

Fig. 6 demonstrates the results of these measurements, along with the frequency response of a conservative bound we used as our noise model, given by

$$W_0 = \frac{1.339e19s + 4.717e25}{s^4 + 1.488e7s^3 + 7.32e14s^2 + 6.936e21s}.$$

Fig. 7 demonstrates the corresponding Pound–Drever–Hall detector (output) signal for one experiment, as well as for the ensemble average over all 30 experiments. Note the resonant spike corresponding to the equilibrium frequency of the laser locked to the high fidelity optical cavity of the Pound–Drever–Hall mechanism. Equipped with these models of the laser system and its corresponding frequency-weighted noise distribution, we are now prepared to begin systematic validation experiments and controller design.

IV. Validation and Controller Design

The process for experimentally verifying our black-box models of the system was relatively simple. Essentially, since all measurements on the system had to be closed-loop measurements, our options were to use the identified models to design other stabilizing controllers with wildly different closed-loop responses and then compare the theoretical response of the models with the experimental response of the implemented system. Discrepancies between theoretical or simulated response and experiment could be attributed to modeling error, provided we did not make a mistake when implementing the intended controller design. To protect against this possibility, we also directly and separately measured the response of the controller to verify that the implementation was, in fact, behaving as designed. That is, for each controller, we verified

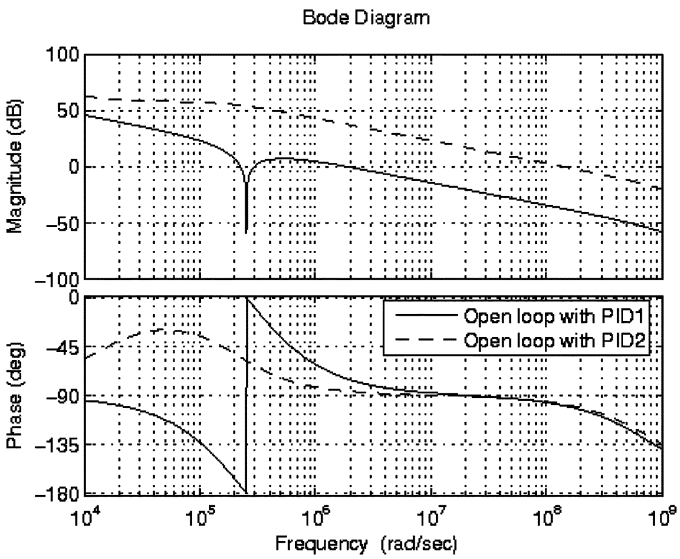

Fig. 9. Open-loop bode plots of P_0K with P_0 being the second-order model. This figure illustrates the high open-loop gain of PID2 relative to PID1. While both controllers are stablizing with respect to the model, PID2 excited unmodeled dynamics and was unstable in practice.

its open-loop response independently from the closed-loop experiments. Thus, experimental discrepancies from theory could confidently be attributed to unmodeled dynamics of the laser system and not to the controller.

A key limitation in this process, however, was the fact that the feedback controllers were all implemented in analog circuitry, so changing controllers with very different structure would result in significant implementation costs. As a result, we were restricted to designing PID controllers with the following structure:

$$K = K_t\left(K_p + \frac{K_i}{s} + \frac{K_d s}{s+\tau_d}\right).$$

Moreover, we were further restricted by our desire to measure the response of the controller directly. As a result, we needed to introduce a limiting resistor on the integrator in order to keep low frequency gains at a reasonable level when independently measuring the controller's open-loop response. Thus, although we would implement the PID controller with structure as given above in the closed-loop system, we would validate a perturbation of the controller itself by introducing the resistor τ_i corresponding to the following structure:

$$K_m = K_t\left(K_p + \frac{K_i}{s+\tau_i} + \frac{K_d s}{s+\tau_d}\right).$$

In all our designs $\tau_d \leq 1e9$ and $\tau_i = 3.03e4$.

Fig. 8 shows the results of a validation experiment. We designed a controller, using the indentified black-box models of the system, that would generate a particular resonant frequency and be easy to implement. This response was achieved by removing the proportional control from the existing experimental controller to create PID1 with gains of $K_t = 5.4$, $K_p = 0$, $K_i = 7.0126e3$, $K_d = 94.0171$, and $\tau_d = 8.547e8$. The corresponding transfer function is given by

$$\text{PID1} = \frac{0.8471s^2 + 63.18s + 5.4e10}{0.001669s^2 + 1.426e6s}.$$

Measuring the closed-loop gains from d to e of sinusoidal disturbances at 30 distinct frequencies, the plot compares these experimental values with the theoretical response of the system using both the second-order model and the fourth-order model [see Fig. 8(a)]. Moreover, we compare the experimental and theoretical response of the controller in Fig. 8(b). Noting that the controller appears to be implemented well, then we conclude that models are good descriptions of the actual system up to about $\omega = 10^6$, after which high frequency unmodeled dynamics appear to be present in the system.

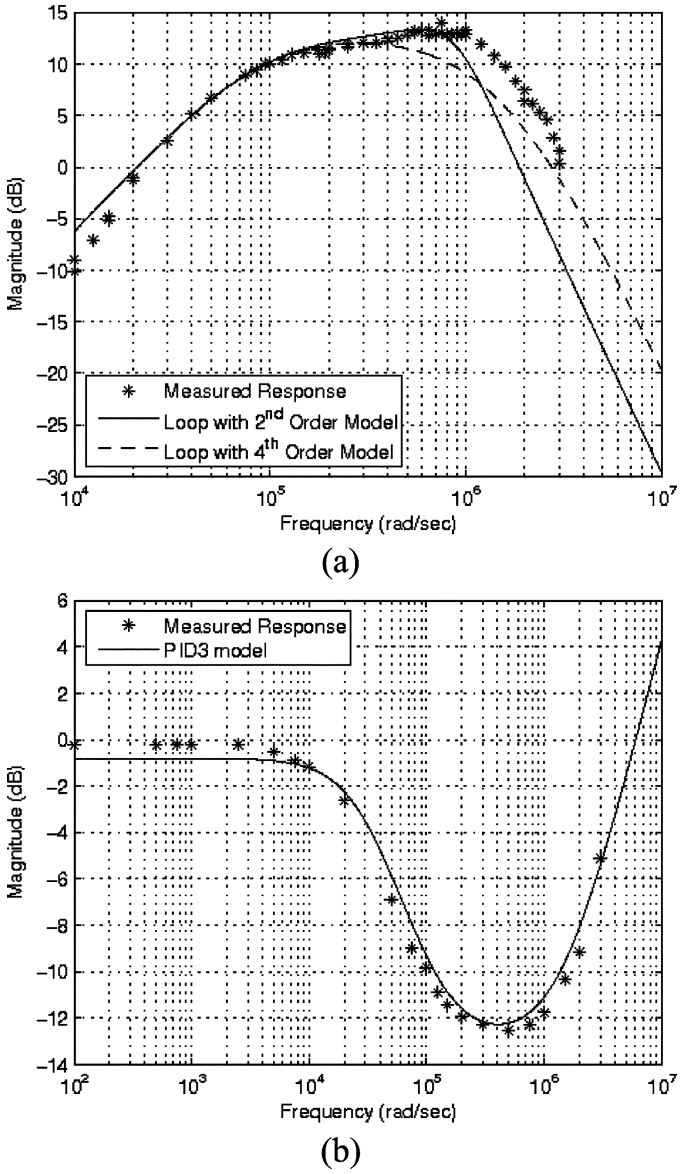

Fig. 10. Measurements with comparisons to our models for $PID3$. (a) Closed-loop Bode plot from d to e of both models with $K = \text{PID3}$. (b) Open-loop Bode plot of the model of PID3 compared with measured values of the open loop response of the actual controller.

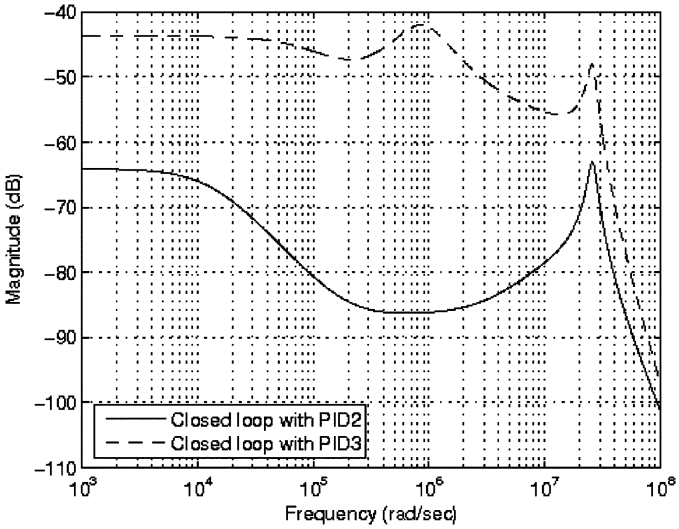

Fig. 11. Comparison of the theoretical noise attenuation performance of PID2 and PID3. We show the closed-loop bode plot comparison from n to e using the second-order model of the system. PID3 sacrifices nominal performance in order to avoid unmodeled dynamics and gain robust stability.

To test how strongly the presence of these high frequency unmodeled dynamics would affect controller design, we next consider a controller that excites frequencies past $\omega = 10^6$. Such a controller, PID2, is given by $K_t = 5.4$, $K_p = 3.04$, $K_i = 3.94e4$, $K_d = 8.09e3$, with $\tau_d = 1e9$, with transfer function

$$\text{PID2} = \frac{4.371e4s^2 + 1.639e10s + 2.13e14}{s^2 + 1e9s}.$$

Fig. 9 demonstrates the open-loop gain PK for PID2 compared with those for PID1. Note that PID2 exhibits high gain at frequencies well beyond $\omega = 10^6$. If either of the black-box second- and fourth-order models were perfect, PID2 would stabilize the system. Moreover, the performance of the closed-loop system in terms of noise attenuation would be superb. Nevertheless, when we implemented PID2 we found the closed-loop system to be unstable. From this, we learn that the unmodeled dynamics beyond $\omega = 10^6$ are not benign and should not be excited in a working control design.

Having validated our models of the laser system and having developed some understanding of their limitations past frequencies of $\omega = 10^6$, we finally consider the design of a working controller. The primary objective of the controller is to attenuate noise as much as possible. Nevertheless, in doing so we recognize that we are constrained by our desire not to excite the unmodeled dynamics in the system. Such a controller is given by PID3 with gains $K_t = 5.4$, $K_p = 0.0443$, $K_i = 3.778e3$, $K_d = 25.6410$, with $\tau_d = 8.547e8$ and transfer function

$$\text{PID3} = \frac{0.4296s^2 + 6.333e5s + 5.4e10}{0.003097s^2 + 2.647e6s}.$$

Fig. 10(a) compares the theoretical and experimental closed-loop responses from d to e, while Fig. 10(b) presents the results of the controller validation experiments. Note in part a that the closed-loop response is rolling off rapidly after $\omega = 10^6$, thus respecting our constraint not to excite the unmodeled dynamics and preserve stability. Nevertheless, we note in Fig. 11 that the noise attenuation of PID3 is substantially worse than that which would be theoretically possible for PID2. This leads us to the conclusion that this deterioration in performance is necessary to preserve system stability, given the coarse understanding of our system captured in our black-box models and our constraints on admissible controller structure. To achieve better performance, we would need to either relax our implementation constraints on the PID structure of the controllers, allowing, for example, more advanced control techniques, or we would need invest in the development of higher fidelity models of the laser system to understand dynamics of the system beyond frequencies $\omega = 10^6$.

V. Conclusion

In this study, we have explored the identification and control of a grating-stabilized external-cavity diode laser using a Pound–Drever–Hall mechanism to generate an error signal comparing the actual laser output with a desired reference wavelength. We used black-box identification techniques due to the complexity of our system and the absence of first-principle models. The identification process was necessarily closed-loop because of nonlinear effects associated with the Pound–Drever–Hall mechanism as an error sensor. Nevertheless, we obtained two linear models of the laser system that captured the prominent dynamics up to about 10^6 rad/s. Moreover, we characterized the frequency response of the resulting model discrepancy to use as a noise model to help guide feedback design. We then validated these models by designing new controllers and comparing the theoretical, simulated response to the actual, experimental response. The first experiment demonstrated the utility of our models up to 10^6 rad/s. The next experiment demonstrated the need to avoid exciting dynamics above 10^6 rad/s by illustrating a controller that was theoretically stabilizing with respect to our models but was, in fact, unstable in practice. Finally, we use this insight to demonstrate the utility of a stabilizing controller that avoids exciting unmodeled dynamics while delivering acceptable noise attenuation for the system.

References

[1] E. D. Black, "An introduction to Pound–Drever–Hall laser frequency stabilization," *Amer. J. Phys*, vol. 69, no. 1, pp. 79–87, Jan. 2001.

[2] R. W. P. Drever, J. L. Hall, F. V. Kowalski, J. Hough, G. M. Ford, A. J. Munley, and H. Ward, "Laser phase and frequency stabilization using an optical resonator," *Appl. Phys. B*, vol. 31, pp. 97–105, 1983.

[3] W. F. Richard, W. O. Chris, and W. H. Leo, "Stabilizing diode lasers to high-finesse cavities," in *Experimental Methods in the Physical Sciences*. San Diego, CA: Elsevier Science, 2002, vol. 40, ch. 1, pp. 1–46.

[4] A. Schoof, J. Grünert, S. Ritter, and A. Hemmerich, "Reducing the linewidth of a diode laser below 30 Hz by stabilization to a reference cavity with a finesse above 10^5," *Opt. Lett.*, vol. 26, no. 20, pp. 1562–1564, Oct. 2001.

[5] H. Stoehr, F. Mensing, J. Helmcke, and U. Sterr, "Diode laser with 1 Hz linewidth," *Opt. Lett*, vol. 31, pp. 736–738, Mar. 2006.

[6] W. Weyerman, B. Neyenhuis, J. Archibald, M. Washburn, D. Durfee, and S. Warnick, "Black-box identification of a grating-stabilized external-cavity diode laser," in *Proc. IEEE MSC*, 2007.

[7] C. E. Wieman and L. Hollberg, "Using diode lasers for atomic physics," *Rev. Sci. Instrum.*, vol. 62, no. 1, pp. 1–20, Jan. 1991.

[8] B. C. Young, F. C. Cruz, W. M. Itano, and J. C. Bergquist, "Visible lasers with subhertz linewidths," *Phys. Rev. Lett.*, vol. 82, no. 19, pp. 3799–3802, May 1999.